Appl. Phys. B 79, 547–554 (2004)
DOI: 10.1007/s00340-004-1612-5

Applied Physics B
Lasers and Optics

A. MARCINKEVIČIUS[1,3,✉]
R. TOMMASINI[1]
G.D. TSAKIRIS[1]
K.J. WITTE[1]
E. GAIŽAUSKAS[2]
U. TEUBNER[3]

Frequency doubling of multi-terawatt femtosecond pulses

[1] Max-Planck Institut für Quantenoptik, Hans-Kopfermann-Strasse 1, 85748 Garching, Germany
[2] Laser Research Center, Vilnius University, Sauletekio av. 10, Vilnius 2054, Lithuania
[3] Institut für Microtechnik Mainz GmbH, Carl-Zeiss-Strasse 18–20, Mainz, Germany

Received: 17 March 2004/Revised version: 2 July 2004
Published online: 11 August 2004 •

ABSTRACT We present an experimental and theoretical study of the influence of the spatial beam quality (fluence and phase distributions) on the second-harmonic generation in KDP crystals pumped by 180-fs pulses at 790 nm. Conversion efficiency and beam focusability are investigated experimentally and theoretically by the numerical analysis of the second harmonic, considering effects due to the cubic nonlinearity, beam diffraction, group-velocity walk-off, and dispersion of the pulses. It was found that the uniform intensity and phase distributions of the fundamental beam are essential to obtain a high focal intensity of the second-harmonic beam.

PACS 42.65.Ky; 42.65.Re

1 Introduction

Terawatt Ti:sapphire laser systems using the chirped-pulse amplification (CPA) technique deliver ultrashort pulses of high peak power which are widely used in the field of high-intensity physics [1]. They suffer from amplified spontaneous emission (ASE) background associated with the main pulse and pre- and post-pulses. In solid–target interaction experiments at high intensities, such pre-pulses and the ASE create a low-density plasma prior to the main pulse and thus significantly alter the physics of the light–matter interaction, especially for high-order harmonic generation from solid targets [2, 3], isochoric heating [4], and ion-acceleration experiments [5, 6] from thin foils. Second-harmonic generation (SHG) of femtosecond pulses can improve the intensity contrast of laser pulses.

However, group-velocity mismatch (GVM) between the fundamental and generated second-harmonic (SH) pulses affects the efficiency of SHG with ultra-short laser pulses. Therefore, thin crystals and high-intensity pulses are preferable for efficient SH generation. On the other hand, at high intensities the local refractive index of the crystal changes with the laser intensity, primarily because of the third-order nonlinear susceptibility, affecting the spatial characteristics of the laser beam. Self-phase modulation (SPM) and cross-phase modulation (XPM) are of particular concern for SH spectral broadening above the Fourier-transform limit due to the high intensity and short duration of the pulses. When an intense laser pulse propagates through a medium, its phase and amplitude can change due to SPM. Additionally, when the fundamental and SH waves simultaneously propagate in a condensed medium, they nonlinearly couple through cross-phase modulation, whereby further phase and amplitude modulations are introduced. These effects degrade the beam quality and also influence both the conversion efficiency and the focusability of the SH beam.

A number of groups have investigated SHG with intense femtosecond laser pulses with intensities exceeding 100 GW/cm^2. Chien et al. [7] reported an energy-conversion efficiency of 80% for 4-mm-thick type I potassium dideuterium phosphate (KDP) crystals using 500-fs, 1053-nm laser pulses at an intensity as high as 400 GW/cm^2. Krylov et al. [8] investigated SHG with type I KDP crystals for different crystal thicknesses of 3, 5, 10, and 40-mm, respectively, using 150-fs, 780-nm laser pulses at an intensity of about 150 GW/cm^2. They concluded that the energy-conversion efficiency could not exceed 50% due to the modulation of the phase of the fundamental pulse and this effect could be even larger than that due to group-velocity mismatch. Neely et al. [9] investigated frequency conversion of intense picosecond laser pulses with 4-mm- and 2-mm-thick KDP crystals. They obtained conversion efficiencies as high as 60% and also observed a multi-foci structure of the SH far-field intensity distribution due to the thickness of the crystal and the high intensity. Queneuille et al. [10] discussed improvement of SH focusability by wavefront correction after SHG with a deformable mirror. They obtained an energy-conversion efficiency of approximately 55% for a 4-mm-thick type I KDP crystal using 400-fs, 1053-nm laser pulses at an intensity of about 200 GW/cm^2. After SH wavefront correction, they were able to reach a focal intensity of 10^{19} W/cm^2 with an estimated intensity-contrast ratio of 10^{-9}. More recently, Aoyama et al. [11], by pre-compensating the phase shift due to the third-order susceptibility $\chi^{(3)}$ as proposed by Ditmire et al. [12], were able to reach 80% conversion efficiency for 130-fs laser pulses at an intensity of 190 GW/cm^2.

In most of the numerous investigations of frequency conversion with picosecond or sub-picosecond laser pulses, the

✉ Fax: +49-89/32905-200, E-mail: andrius@mpq.mpg.de

biggest concern has been the achievement of high conversion efficiencies. On the other hand, for the experiments in high-field physics, high-contrast femtosecond pulses with a nearly diffraction limited focus are needed. Factors limiting the focusability of frequency-doubled multi-terawatt laser pules have still not been quantitatively investigated. To the best of our knowledge, only two groups [9, 10] have addressed SH focal intensity distributions.

In this paper, we investigate the frequency conversion with a 2-mm-thick KDP crystal and high-intensity laser pulses provided by the 2-TW, 130-fs and 10-TW, 180-fs output beams from the 10-Hz ATLAS (Advanced Titanium:Sapphire Laser) facility at the Max-Planck Institute for Quantum Optics (MPQ) in Garching, Germany. SHG with the 2-TW ATLAS beam allowed us to reach peak intensities of about $8 \times 10^{18}\,\mathrm{W/cm^2}$ and an intensity-contrast ratio of about 10^{-9}. We will give a comprehensive comparison of second-harmonic focal intensities obtained with 2-TW and 10-TW laser pulses. The experimental results are compared with theoretical ones by taking into account group-velocity dispersion, pulse walk-off, and self-phase modulation in the strongly nonlinear regime. The influence of the pump-beam modulations in space and phase, as well as phase modulations induced by the third-order nonlinearity, on the focal intensity distribution are shown.

2 Theoretical background

The detailed spectral and angular characteristics of the broadband femtosecond pulses are important issues in frequency conversion. The phase and amplitude modulations of the pulse due to both second- and third-order nonlinearities are expected to modify the spectra and angular distributions of the interacting fields. The equations that describe the three-wave nonlinear interaction are well known and can be derived from Maxwell's equations using the common slowly varying amplitude approximation [13]. To take into consideration the above-mentioned effects, terms describing diffraction of the beams as well as dispersive spreading have to be included. It is necessary to mention here that, for our experimental conditions, the beam diffraction plays an insignificant role.

Using the plane-wave approximation, the electric fields of the pulses are represented as interacting plane waves having central frequencies $\omega_1, \omega_2 = 2\omega_1$ with corresponding wave vectors $\boldsymbol{k}_1, \boldsymbol{k}_2$:

$$\begin{aligned}\boldsymbol{E}_1(\boldsymbol{r},t) &= \frac{1}{2}A_1(\boldsymbol{r},t)\exp\left[\mathrm{i}(\omega_1 t - \boldsymbol{k}_1\boldsymbol{r})\right] + \text{c.c.}\,,\\ \boldsymbol{E}_2(\boldsymbol{r},t) &= \frac{1}{2}A_2(\boldsymbol{r},t)\exp\left[\mathrm{i}(2\omega_1 t - \boldsymbol{k}_2\boldsymbol{r})\right] + \text{c.c}\,,\end{aligned} \tag{1}$$

where $\boldsymbol{k}_i = \omega_i/n_i c$ $(i = 1, 2)$ are the propagation constants, n_i is the refractive index for the ith wave, and c is the vacuum speed of light. Subscripts 1 and 2 here refer to the fundamental and SH pulses, respectively. Substituting (1) into the expression for the nonlinear polarization up to the third order,

$$P^{(\mathrm{NL})}(\boldsymbol{r},t) = \chi^{(2)}E^2(\boldsymbol{r},t) + \chi^{(3)}E^3(\boldsymbol{r},t)\,, \tag{2}$$

and keeping only the terms involving the fundamental or SH carrier frequencies, the contributions to the (non-resonant) nonlinear polarization waves become

$$\begin{aligned}&P_1^{(\mathrm{NL})}(\boldsymbol{r},t)\\ &= \frac{1}{2}\left[\chi^{(2)}A_1A_2^* + 3\chi^{(3)}\left(|A_1|^2 + 2|A_2|^2\right)A_1\right]\mathrm{e}^{\mathrm{i}\boldsymbol{k}_1\boldsymbol{r}-\mathrm{i}\omega_1 t} + \text{c.c.}\,,\end{aligned} \tag{3}$$

$$\begin{aligned}&P_2^{(\mathrm{NL})}(\boldsymbol{r},t)\\ &= \frac{1}{2}\left[\chi^{(2)}A_1A_2^* + 3\chi^{(3)}\left(|A_2|^2 + 2|A_1|^2\right)A_2\right]\mathrm{e}^{\mathrm{i}\boldsymbol{k}_2\boldsymbol{r}-\mathrm{i}2\omega_1 t} + \text{c.c}\,.\end{aligned} \tag{4}$$

The $\chi^{(2)}$ nonlinearity gives rise to the parametric gain (or depletion) of the fundamental and SH pulses, the $\chi^{(3)}$ nonlinearity to self-phase modulation effects, and the combined action of the $\chi^{(2)}$ and $\chi^{(3)}$ nonlinearities is responsible for the cross-phase modulation effects.

The use of the slowly varying envelope approximation yields the following equations for the coupled propagation of the fundamental and SH waves in the frame moving with the pump pulse [13]:

$$\begin{aligned}&\frac{\partial A_1}{\partial z} - \frac{\mathrm{i}}{2k_1}\left(\frac{\partial^2 A_1}{\partial x^2} + \frac{\partial^2 A_1}{\partial y^2}\right) + \nu_{12}\frac{\partial A_1}{\partial t} + \mathrm{i}d_1\frac{\partial^2 A_1}{\partial^2 t}\\ &= \mathrm{i}\frac{\omega_1\chi^{(2)}}{2n_1c}A_2A_1^*\exp(-\mathrm{i}\Delta kz) + \mathrm{i}\frac{3\omega_1\chi^{(3)}}{4n_1c}\left[|A_1|^2 + 2|A_2|^2\right]A_1,\end{aligned} \tag{5}$$

$$\begin{aligned}&\frac{\partial A_2}{\partial z} - \frac{\mathrm{i}}{2k_2}\left(\frac{\partial^2 A_2}{\partial x^2} + \frac{\partial^2 A_2}{\partial y^2}\right) + \mathrm{i}d_2\frac{\partial^2 A_2}{\partial^2 t}\\ &= \mathrm{i}\frac{\omega_2\chi^{(2)}}{2n_2c}A_1^2\exp(\mathrm{i}\Delta kz) + \mathrm{i}\frac{3\omega_2\chi^{(3)}}{4n_2c}\left[2|A_1|^2 + |A_2|^2\right]A_2\,,\end{aligned} \tag{6}$$

where $\Delta\boldsymbol{k} = \boldsymbol{k}_2 - 2\boldsymbol{k}_1$ is the wave-vector phase mismatch, $1/\nu_{12} = [\partial k_1(\omega)/\partial\omega]^{-1} - [\partial k_2(\omega)/\partial\omega]^{-1}$ is the group-velocity mismatch of the SH with respect to the fundamental wave, and $d_i = 0.5(\partial^2 k/\partial\omega^2)|_i$ $(i = 1, 2)$ is the group-velocity dispersion (GVD) coefficient. In the case of type I SHG in KDP, the group-velocity walk-off rate between the fundamental pulse at 800 nm and the SH is 77 fs/mm [12].

The system of (5) and (6) was solved numerically by using the common split-step procedure dividing the equation into dispersive and nonlinear parts. We have solved them using the fast Fourier transform and fourth-order Runge–Kutta procedures for each (dispersive and nonlinear) step, respectively [14, 15]. The field amplitude $A_0(x, y, 0, t)$ at the entrance of the nonlinear medium was taken in the form of a plane-wave Gaussian envelope in time with lateral distribution $A_0(x, y) = \sqrt{8\pi I_0(x, y)/c}$, where $I_0(x, y)$ is the experimentally measured beam intensity. Pump pulses of 180-fs duration propagating in 2-mm-thick type I KDP crystal are used in the calculations.

3 Experimental setup

The experiments were performed with the two different versions of the ATLAS facility. The 2-TW version (ATLAS-2) delivers 130-fs long pulses, with an energy of up to 230 mJ, a bandwidth of 8 nm, and a central wavelength of

792 nm. The pulse-contrast ratio at 792 nm was about $1:10^8$ at $t > 2$ ns and $1:10^4$ at 1 ps $< t < 2$ ns.

In the ATLAS-10 configuration, the 330-mJ pulses from ATLAS-2 (before compression) are further amplified in the second multi-pass amplifier using four passes in a 40-mm Ti:sapphire crystal to an energy of ~ 1.3 J and then compressed in a second vacuum compressor to pulses of about 700 mJ/180 fs with a bandwidth of 6 nm and a central wavelength of 793 nm. The pulse contrast at the fundamental wavelength was somewhat poorer than that in ATLAS-2, being $1:5\times10^7$ at $t > 2$ ns and $1:10^3$ at 1 ps $< t < 2$ ns. To correct the strong wavefront distortions and intensity-profile modulations induced by growth defects of the second multi-pass amplifier, we use two deformable bimorph mirrors [16]. These allow us to reduce the intensity modulations by more than a factor of three and minimize the wavefront peak-to-valley variations to $\lambda/4$.

The experimental setup used in the SHG experiments is depicted in Fig. 1. SHG was performed using two different 2-mm-thick, type I KDP crystal plates (wavefront distortion $\lambda/8$ at 790 nm) with the clear aperture of 65 mm for ATLAS-10 and 55 mm for ATLAS-2 and which were placed in an evacuated tube system. To reduce the group-velocity mismatch, we increased the pulse duration of ATLAS-2 to 180 fs by detuning the compressor. For separation of the second harmonic from the unconverted fundamental, four dielectric mirrors (M1–M4 in Fig. 1), reflecting $> 99\%$ of SH light and transmitting $> 99\%$ of the fundamental light, were used. This results in a suppression ratio of about 10^8 for the fundamental. For the ATLAS 2 experiments, these mirrors as well as the $\lambda/2$ plate (not shown in Fig. 1) were placed not in vacuum but in air, so the SH beam is transmitted through two 3-mm-thick antireflection-coated fused-silica windows on the exit of the beamline and on the entrance of the target chamber. For the ATLAS-10 measurements, they were part of the vacuum beamline and high optical quality mirrors M1–M4 were used in order to maintain the flat wavefront (surface flatness typically $\lambda/8$). For the polarization rotation, instead of using a $\lambda/2$ plate, we implemented a periscope with mirrors M1 and M2. Using color filters and a calibrated PIN photodiode, we verified that in both SHG schemes fundamental light was suppressed below our detection limit of 0.1 nJ. In the vacuum chamber, the laser light was reflected by the 99% reflection dielectric mirror, M5, and focused by the dielectric off-axis parabolic mirror, OAP, with f-number $F^{\#} = f/2.5$ (Fig. 1). Beam leaking through mirror M5 was used for the monitoring of the input laser energy with a calibrated PIN photodiode or the measurement of the SH spectrum with a spectrograph (ORIEL, MS125) equipped with a 1200-grooves/mm grating. The inverse linear dispersion of this spectrograph was 0.7 nm/mm at 400 nm, i.e. the spectral resolution was around 0.07 nm for the entrance slit of 100-μm width.

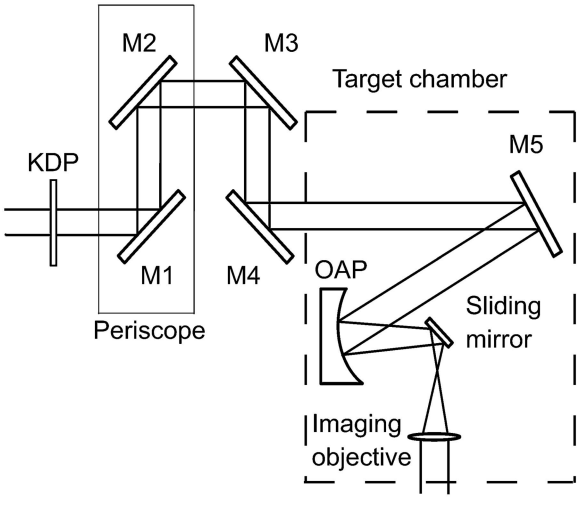

FIGURE 1 Experimental setup for SHG and SH far-field measurements. The laser pulse is frequency doubled in the KDP crystal and then selected from the fundamental wavelength by four dichroic mirrors M1–M4. The OAP $f/3$ off-axis parabola is used for SH far-field measurements

The second-harmonic focus was checked using a small gold pickup mirror which could be inserted into the beam just before the parabola focus and which deflected the beam through an $F^{\#} = f/2$ imaging lens onto a 14-bit CCD camera. For the ATLAS-2 SH focus diagnostics, we used a magnification factor of 55, whereas for ATLAS-10 the magnification was 65. In some ATLAS-10 SHG experiments, we replaced the M5 mirror by an un-coated glass wedge in order to measure the focal intensity distribution with the maximally possible SH pulse energy.

The intensity distributions of the fundamental beam were registered by the 14-bit CCD camera at the position of the nonlinear crystal. The SH intensity distributions were captured for ATLAS-2 after mirror M4, and for ATLAS-10 at the position of mirror M3. In the latter case, additional color filters were used to suppress the remaining fundamental beam energy.

4 Experimental results

Experimental conversion efficiencies versus pump intensities are shown in Fig. 2 for both pump sources, ATLAS-2 and ATLAS-10, as solid squares and solid circles, respectively. All experimental points were obtained by averaging over 100 laser shots. The efficiencies increase monotonically with the pump intensity when it is between 10 and 40 GW/cm^2 for the ATLAS-2 beam, and 30 and 120 GW/cm^2 for the ATLAS-10 beam. The efficiency reaches its maximum at 50 GW/cm^2 and 200 GW/cm^2 for the ATLAS-2 and ATLAS-10 beams, respectively. In the case of ATLAS-10, a further increase in the pump intensity does not significantly change the conversion efficiency due to a possible reduction of the phase-matching bandwidth and the phase modulation caused by the SPM at high intensities leading to saturation of the conversion efficiency [17, 18]. The absence of a drop in the conversion efficiency with increasing pump intensity indicates that there is no significant reconversion from the second harmonic into the fundamental due to the cubic nonlinearity $\chi^{(3)}$ [12]. The different slopes of the conversion efficiency for the ATLAS-2 and ATLAS-10 beams possibly can be explained by taking into account that (i) different KDP crystals with possibly different nonlinear coefficients were used, (ii) different pedestal intensities of the fundamental were present [19], and (iii) two beams with different phase abberations were used as the pump (see discussion below). The

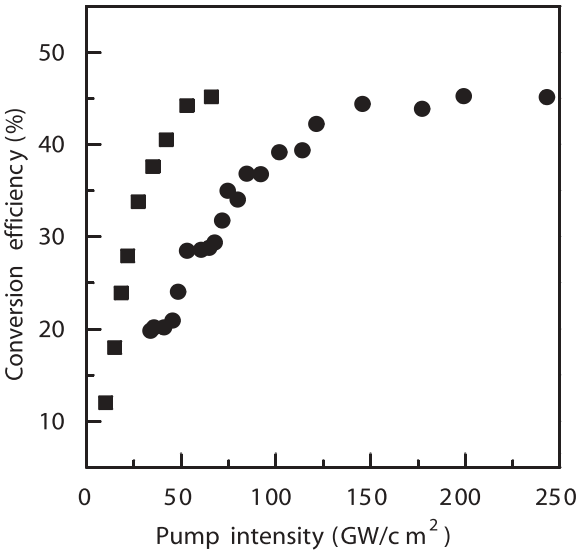

FIGURE 2 Second-harmonic conversion efficiencies for the ATLAS-2 beam (*solid squares*) and for the ATLAS-10 beam (*solid circles*)

influence of each factor on the conversion efficiencies are the subject of separate investigations.

Measured second-harmonic spectra for the maximal fundamental intensities from ATLAS-2 and ATLAS-10 are presented in Fig. 3 as solid squares and solid circles, respectively. The smooth spectrum registered at the incident intensity of 50 GW/cm^2 (solid squares in Fig. 3) indicate that no spectral modulation is introduced by self-phase modulation. Slight modulations appeared in the ATLAS-10 second-harmonic spectrum when the incident intensity reached 250 GW/cm^2 and the maximal conversion efficiency was observed. SH spectral widths of 1.8 nm for low incident intensity and 1.7 nm for high incident intensity were in good agreement with the calculated value of about 1.7 nm for the 2-mm-thick KDP crystal. The shift of the ATLAS-10 SH central wavelength is caused by the red shift of the ATLAS-10 fundamental spectrum in the second multi-pass amplifier.

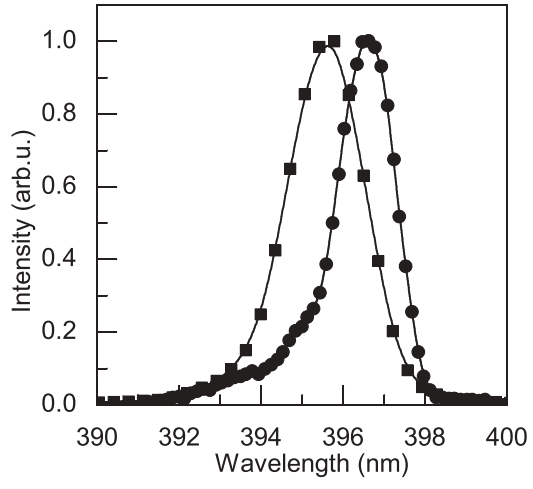

FIGURE 3 Spectra of the second harmonic generated with ATLAS-2 (*squares*) and ATLAS-10 (*circles*) pulses of 50 and 250 GW/cm^2, respectively

In order to investigate the intensity distribution at the focus of the OAP, i.e. in the far field, information about the near-field intensity distribution is necessary. Captured intensity distributions of the ATLAS-2 fundamental and second harmonic at maximal pump intensity are presented in Fig. 4a and b, respectively. The fundamental beam diameter was about 63 mm (at 86.5% level) and that of the second harmonic was 60 mm. The diffraction-limited focus diameter of our OAP should then be $d = 2.44\lambda\ F^{\#} = 2.66\ \mu$m (for the Airy-disk pattern). The circular fringe pattern in the fundamental beam intensity distribution originates from beam clipping at the input window of the ATLAS-2 pulse compressor, and this pattern is transferred to the SH intensity distribution (Fig. 4b).

A magnified intensity distribution of the second-harmonic focus obtained with the OAP is presented in Fig. 5. The focal spot mainly consists of a single peak containing 50% of the total energy within a 2.4-μm-diameter area (see inset in Fig. 5, approximately 6 μm for the Airy-disk pattern), i.e. the spot size is approximately two times diffraction limited. This leads to an average intensity of 2×10^{18} W/cm^2, with a peak intensity of about 8×10^{18} W/cm^2. This indicates that the spatial phase distribution across the ATLAS-2 SH beam is almost uniform and was not affected by propagation in air for more than 1 m. Furthermore, from the pulse-contrast ratio at the fundamental wavelength, the contrast ratio of the second harmonic was estimated to be $1 : 10^{16}$ at $t > 2$ ns, and $1 : 10^8$ in the interval 1 ps $< t <$ 2 ns, at fundamental intensities < 50 GW/cm^2.

Similarly, we registered the intensity distributions of ATLAS 10 at the fundamental wavelength and second harmonic (Fig. 6a and b, respectively). These images were taken using the minimally possible pump intensity because of propagation through glass windows. Strong modulations in the intensity spatial distribution and wavefront distortions due to amplifier crystal-growth defects and pump-induced modulations were minimized using two deformable mirrors as described by Baumhacker et al. [16]. Several hot spots in the fundamental intensity distribution are still clearly observable; nevertheless, the intensity modulation was reduced by a factor of two. As one would expect, the SH intensity modulation was even larger (Fig. 6b) due to operation in the linear conversion regime. The fundamental beam diameter after propagation in vacuum of about 10 m downstream from the second deformable mirror was about 67 mm (at 86.5% level) and the second-harmonic beam diameter was 68 mm. It should be pointed out that, due to technical restrictions, the second-harmonic intensity distribution was registered after a propagation distance of 6 m from the position where the fundamental intensity distribution was registered.

Magnified intensity distributions of the second-harmonic focus obtained with the OAP are presented in Fig. 7a–d. Due to the potential application for the high-order harmonic generation, we examined the SH focal intensity distributions using pump intensities at 2 (a, b) and 250 GW/cm^2 (c, d). In the first case, the conversion efficiency depends linearly on intensity and in the second case it is in the saturation regime. As can be seen from vertical lineouts in Fig. 7b and d, the central peak in the focal intensity distribution is surrounded by a broad halo, which becomes more pronounced with increasing pump intensity. For 250 GW/cm^2 pump, 50% of the

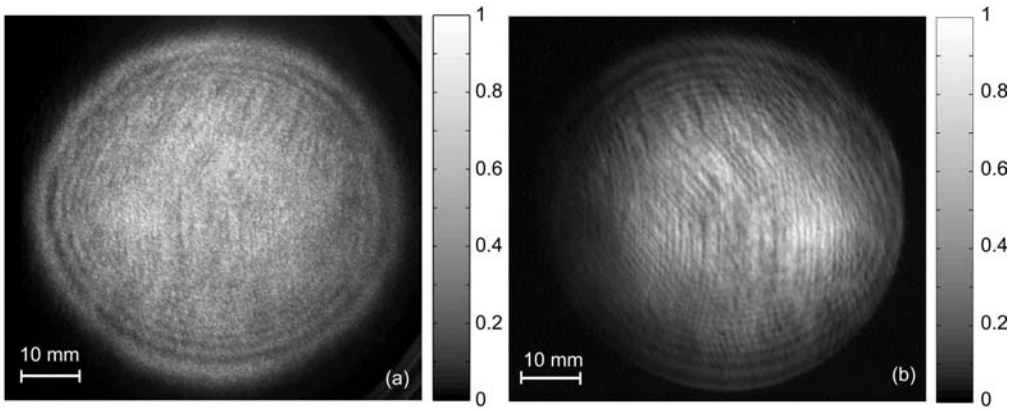

FIGURE 4 Intensity distributions of ATLAS-2 fundamental (**a**) and second harmonic (**b**) at a fundamental intensity of 40 GW/cm^2

energy was concentrated within a 14-μm-diameter area, i.e. in an area which is approximately four times bigger than the diffraction-limited spot. This leads to a peak intensity of about 3.2×10^{18} W/cm^2. The contrast ratio of the ATLAS-10 second-harmonic pulse was estimated to be $1 : 10^{14}$ at $t > 2$ ns, and $1 : 10^6$ at 1 ps $< t <$ 2 ns, at fundamental intensities < 120 GW/cm^2.

To understand why the focal intensity is so low, one should remember that for obtaining a high focal intensity an excellent phase distribution over the beam is necessary. If we assume that the phase of the fundamental beam entering the SH crystal is constant, then it is reasonable to expect that the SH beam phase variations were induced by the third-order nonlinearity in the crystal due to strong intensity modulations. Using the theoretical model described in Sect. 2, we were able to calculate the intensity and phase distributions of the SH at the output of the nonlinear crystal. In these calculations, we assumed a phase mismatch $\Delta k = 0$, a constant phase, and used experimentally obtained fundamental intensity distributions at the crystal position as the input to the code. First, we calculated the intensity and phase distributions for ATLAS 2, presented in Fig. 8a and b, respectively. For these, we used the pump intensity distribution depicted in Fig. 4a. From the comparison of the calculated SH intensity distribution (Fig. 8a) with that experimentally registered (Fig. 4b), we can conclude

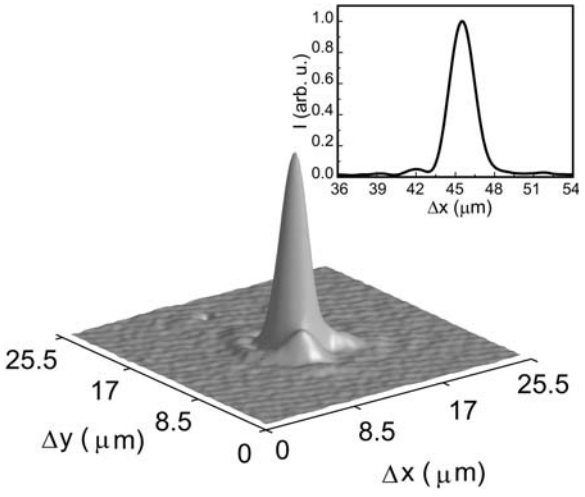

FIGURE 5 Magnified ATLAS-2 second-harmonic focal intensity distribution at a fundamental beam intensity of 200 MW/cm^2

that these patterns are in reasonably good agreement. The calculated SH phase distribution was relatively constant, particularly in the central part of the beam. The phase variation over the whole beam was about 0.1λ (0.19π rad), primarily due to the presence of diffraction rings in the fundamental beam intensity distribution.

Similar calculations were performed using the ATLAS-10 pump beam (Fig. 6a) as an input. The resulting SH intensity and phase spatial distributions are presented in Fig. 9a and b, respectively. As can be seen from Fig. 9a, even for a strongly modulated fundamental beam, the calculated intensity distribution closely resembles the experimentally registered one (Fig. 6b). The phase variation over the whole beam is more than three times larger than that in the ATLAS-2 SH beam, i.e. approximately 0.3λ (0.6π rad). Comparing the positions of the hot spots in the intensity distribution with the positions of the maximal phase variation, we can conclude that the latter were induced in the crystal by the hot spots in the fundamental intensity distribution. This result could explain the distorted focal intensity distribution (Fig. 7b) for a fundamental intensity of 250 GW/cm^2 when the influence of the third-order nonlinearity is not negligible. The phase shift of the whole beam at this intensity will approach unity at the characteristic length of SPM, $L_{\mathrm{SPM}} = \lambda/(2\pi n_0 n_2^{\mathrm{KDP}} I)$, of 0.84 mm. Here we used a value of $n_2^{\mathrm{KDP}} = 4 \times 10^{-16}$ cm^2/W for the nonlinear refractive index of KDP [20]. From this it follows that the focal intensity distribution of the ATLAS-10 SH beam cannot be explained by the modulated fundamental beam only.

The knowledge of the spatial phase of the input laser beam is crucial in determining the quality and the focusability of the second-harmonic beam. In order to evaluate the spatial phase shift across the ATLAS beam, we implemented a numerical iterative phase-retrieval code based on a generalized [22] Gerchberg–Saxton algorithm [21] in the form reported in [23] (see Eqs. (16)). In our specific case, the algorithm allows the retrieval of the spatial phase shift across the beam in two different (x, y) directions, normal to the propagation axis z (z planes), once we know the corresponding intensities, and thus the amplitudes. The spatial distribution of the intensity of the ATLAS beam was recorded by means of a CCD at two different planes, z_1 and z_2, separated by a few meters propagation distance in an evacuated tube. The propagation distance and CCD resolution were chosen in order to fulfill the Nyquist condition for proper sampling. Assuming a ran-

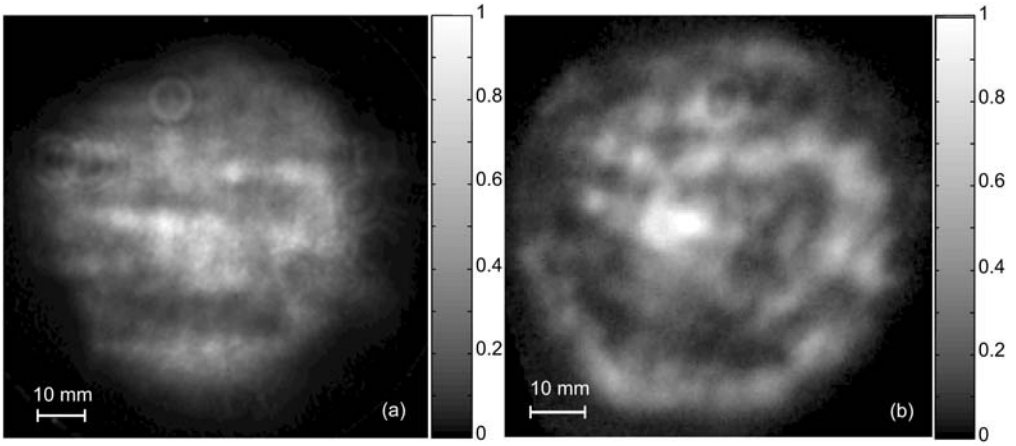

FIGURE 6 ATLAS-10 fundamental (**a**) and SH (**b**) intensity distributions at a fundamental intensity of 1 GW/cm^2

dom array as the initial phase at plane z_1, the code iteratively calculates the spatial phases at the two planes. At each iteration the amplitude of the reconstructed beam, $f_2(x)$, at plane z_2 is compared with the measured amplitude, $f_1(x)$, and the iterative process is terminated as soon as the L_2 distance, $\left[\int (f_1(x) - f_2(x))^2\right]^{1/2}$, is less than 1%.

In phase-retrieval problems, the uniqueness of the solution is always an issue. Let us first notice that in the present case we are mostly interested in the variance of the phase per unit length and thus the issue is not of fundamental importance. In any case, we tested the uniqueness of the solution in the way proposed by Seldin and Fienup [24], i.e. we ran

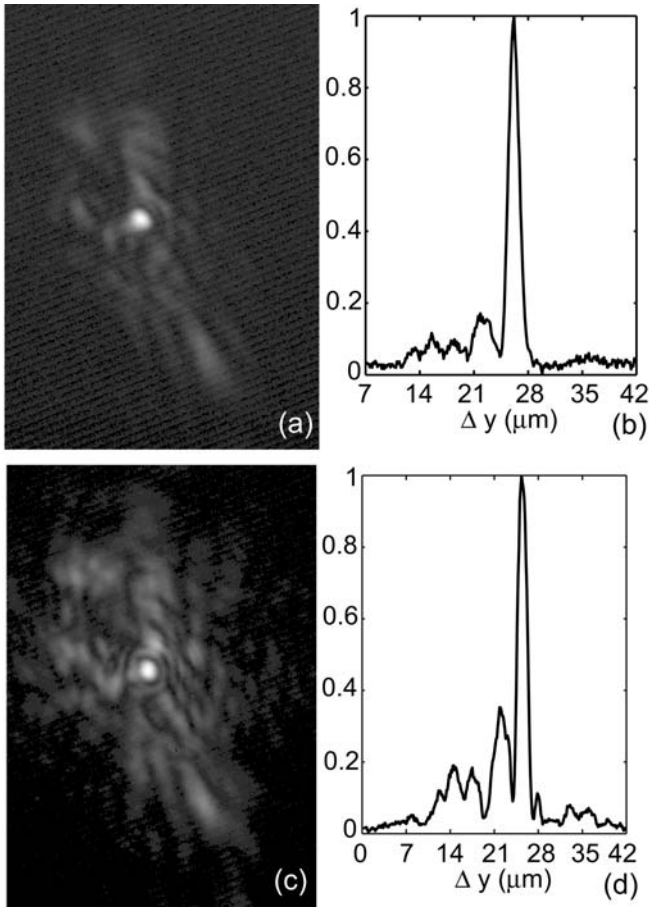

FIGURE 7 Magnified ATLAS-10 SH focal intensity distributions for fundamental intensities of 2 GW/cm^2 (**a**) and 250 GW/cm^2 (**c**). Corresponding vertical lineout cross sections of the intensity distributions are shown in (**b**) and (**d**), respectively

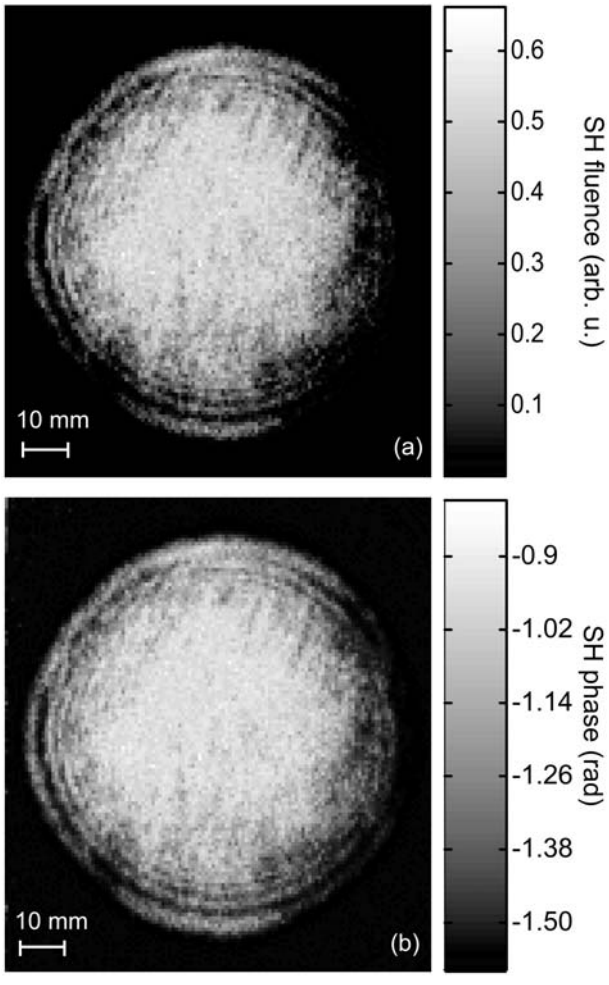

FIGURE 8 Numerical simulations for ATLAS-2 at a fundamental intensity of 30 GW/cm^2: calculated SH intensity distribution (**a**) and phase distribution (**b**)

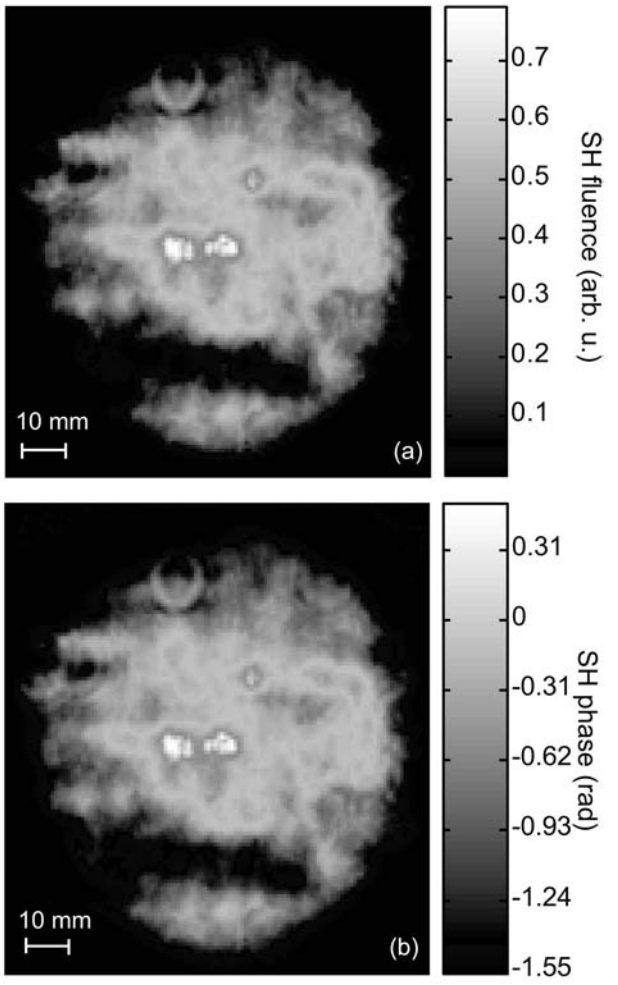

FIGURE 9 Numerical simulations for ATLAS-10 at a fundamental intensity of 200 GW/cm^2: calculated SH intensity distribution (**a**) and phase distribution (**b**)

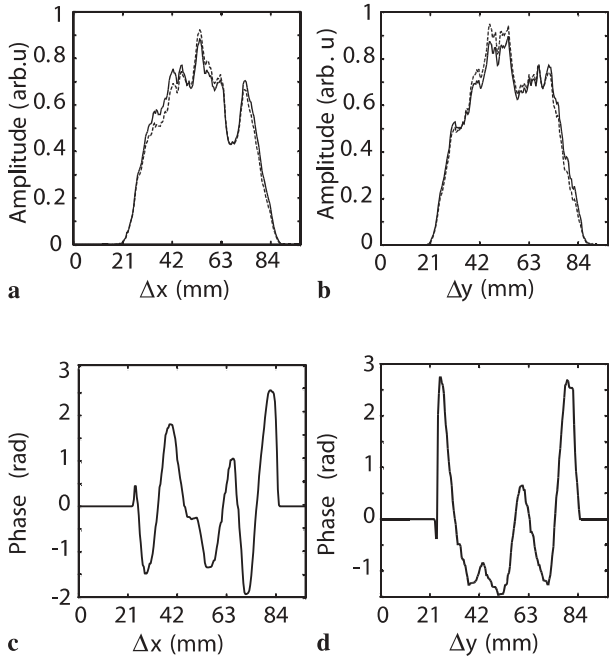

FIGURE 10 Comparison of measured (*solid line*) and calculated (*dotted line*) amplitudes of the electric field of the ATLAS-10 fundamental beam in two orthogonal directions (**a** and **b**). Retrieved spatial phase along the same directions (**c** and **d**)

the code several times each starting from a different array of random numbers as the initial phase and verified that the evaluated phases at the end of the different runs were essentially the same, which means that they differed by less than the 1% L_2-distance value assumed as the convergence criterion. This ensures practical uniqueness of the solution.

Results from our code are shown in Fig. 10. The upper part of the figure shows a comparison of the intensity profiles along the x and y directions for the measured and calculated amplitudes of the beam at the final z_2 plane (Fig. 10a, b solid and dotted lines, respectively). Notice that in order to appreciate a difference in the two amplitudes, we show here the result at an intermediate number of iterations corresponding to a 8% L^2 distance. The lower part of Fig. 10c, d shows the reconstructed phase of the beam in the z_1 plane and at the end of the iterative cycle. As a result, in the central part of the laser beam we obtained average spatial phase variations of about 0.3 λ/cm, which is comparable to the value reported by Baumhacker et al. [16]. Phase distortions in the SH wave will depend approximately linearly on the aberrations of the fundamental wave, $\phi_{\mathrm{SHG}}(x, y) \sim 2\phi_{\mathrm{fund}}(x, y)$ [25]. Thus, even for a low-intensity fundamental wave, phase variations of the SH will be on the order of 0.6 λ/cm and could account for the poor focal intensity distribution (Fig. 7a). Furthermore, phase variations of the fundamental wave cause a variation of the phase-matching angle across the beam and will affect the $\Delta k(x, y)$ distributions, with detrimental effects on the SH intensity distribution and conversion efficiencies (Fig. 2). Hence, more precise control of the ATLAS-10 fundamental beam phase distribution prior to frequency conversion is necessary. Moreover, we can expect an improvement of the SH focal intensity distribution by using an additional deformable mirror placed after the SH crystal.

5 Conclusions

The second-harmonic generation of ∼ 180-fs/790-nm pulses produced by the MPQ ATLAS facility in type I KDP crystals was investigated both theoretically and experimentally. Conversion efficiencies of 45% at a laser intensity of 50 GW/cm^2 were obtained using the ATLAS-2 beam (200-mJ fundamental energy) without substantial degradation of focusabilty. Comparing theoretically calculated intensity and phase distributions for the ATLAS-2 and ATLAS-10 beams (700-mJ fundamental energy) with experimental ones, it was found that the distorted focal intensity distribution of the ATLAS-10 SH beam is most likely caused by an inhomogeneous phase distribution of the fundamental beam, as well as phase changes due to pump intensity modulations inducing considerable phase variations in the SH beam, thereby deteriorating its focal intensity distribution. Hence, to obtain a high SH focal intensity, a fundamental beam without any intensity modulations and spatial phase variations as small as possible is necessary.

ACKNOWLEDGEMENTS We thank A. Böswald and H. Haas for technical support. This work was supported by the European Commu-

nities in the framework of the European–IPP association and the Deutsche Forschungsgemeinschaft (DFG Grant Nos. TE 190/4-1 and TS82/1-1).

REFERENCES

1 A. Pukhov: Rep. Prog. Phys. **66**, 47 (2003)
2 M. Zepf, G.D. Tsakiris, G. Pretzler, I. Watts, D.M. Chambers, P.A. Norreys, U. Andiel, A.E. Dangor, K. Eidmann, C. Gahn, A. Machacek, J.S. Wark, K. Witte: Phys. Rev. E **58**, R5253 (1998)
3 U. Teubner, G. Pretzler, Th. Schlegel, K. Eidmann, E. Forster, K. Witte: Phys. Rev. A **67**, 013816 (2003)
4 A. Saemann, K. Eidmann, I.E. Golovkin, R. Mancini, E. Andersson, E. Forster, K. Witte: Phys. Rev. Lett. **82**, 4843 (1999)
5 M. Roth, A. Blazevic, M. Geissel, T. Schlegel, T.E. Cowan, M. Allen, J.-C. Gauthier, P. Audebert, J. Fuchs, J. Meyer ter Vehn, M. Hegelich, S. Karsch, A. Pukhov: Phys. Rev. Spec. Top. Accel. Beams **5**, 061 301 (2002)
6 M. Kaluza, J. Schreiber, M. Santala, G. Tsakiris, K. Eidmann, J. Meyer ter Vehn, K. Witte: Phys. Rev. Lett. **93**, 045 003 (2004)
7 C.Y. Chien, G. Korn, J.S. Coe, J. Squier, G. Mourou, R.S. Craxton: Opt. Lett. **20**, 353 (1995)
8 V. Krylov, A. Rebane, A.G. Kalintsev, H. Schwoerer, U.P. Wild: Opt. Lett. **20**, 198 (1995)
9 D. Neely, C.N. Danson, R. Allott, F. Amiranoff, J.L. Collier, A.E. Dangor, C.B. Edwards, P. Flintoff, P. Hatton, M. Harman, M.H.R. Hutchinson, Z. Najmudin, D.A. Pepler, I.N. Ross, M. Salvati, T. Winstone: Laser Part. Beams **17**, 281 (1999)
10 J. Queneuille, F. Druon, A. Maksimchuk, G. Cheriaux, G. Mourou, K. Nemoto: Opt. Lett. **25**, 508 (2000)
11 M. Aoyama, T. Harimoto, J. Ma, Y. Akahane, K. Yamakawa: Opt. Express **9**, 579 (2001)
12 T. Ditmire, A.M. Rubenchik, D. Eimerl, M.D. Perry: J. Opt. Soc. Am. B **13**, 649 (1996)
13 Y.R. Shen: *The Principles of Nonlinear Optics* (Wiley, New York 1984)
14 E. Gaižauskas, R. Grigonis, V. Sirutkaitis: J. Opt. Soc. Am. B **19**, 2957 (2002)
15 J. Zhang, J.Y. Huang, H. Wang, K.S. Wong, G.K. Wong: J. Opt. Soc. Am. B **15**, 200 (2002)
16 H. Baumhacker, G. Pretzler, K.J. Witte, M. Hegelich, M. Kaluza, S.A. Kudryashov, V. Samarkin, A. Roukossouev: Opt. Lett. **27**, 1570 (2002)
17 R.C. Eckardt, J. Reintjes: IEEE J. Quantum Electron. **20**, 1178 (1984)
18 D. Kuhlke, U. Herpers: Opt. Commun. **69**, 75 (1988)
19 E. Gaizauskas, R. Grigonis, V. Sirutkaitis, A. Piskarskas, S. Kohlweyer, G.D. Tsakiris: Lith. J. Phys. **36**, 307 (1996)
20 R. Adair, L.L. Chase, S.A. Payne: Phys. Rev. B **39**, 3337 (1989)
21 R.W. Gerchberg, W.O. Saxton: Optik **35**, 237 (1972)
22 G. Yang, B. Dong, B. Gu, J.-Y. Zhuang, O.K. Ersoy: Appl. Opt. **33**, 209 (1994)
23 R. Tommasini, F. Lowenthal, J.E. Balmer, H.P. Weber: Opt. Commun. **153**, 339 (1998)
24 J.H. Seldin, J.R. Fienup: J. Opt. Soc. Am. A **7**, 412 (1990)
25 J. Hou, Y. Zhang, W. Jiang, N. Ling: J. Opt. Soc. Am. B **19**, 1380 (2002)